Proceedings of 2018 ASME/Bath Symposium on Fluid Power and Motion Control
FPMC 2018
Septemebr 12-14, 2018, University of Bath, Bath, United Kingdom

FPMC2018-8900

HIGH FIDELITY DYNAMIC MODELING AND CONTROL OF POWER REGENERATIVE HYDROSTATIC WIND TURBINE TEST PLATFORM

Biswaranjan Mohanty
Department of Mechanical Engineering
University of Minnesota
Minneapolis, MN 55455
Email: mohan035@umn.edu

Kim A Stelson
Department of Mechanical Engineering
University of Minnesota
Minneapolis, MN 55455
Email: kstelson@umn.edu

ABSTRACT

Conventional wind turbines are equipped with multi-stage fixed-ratio gearboxes to transmit power from the low speed rotor to the high speed generator. Gearbox failure is a major issue causing high maintenance costs. With a superior power to weight ratio, a hydrostatic transmission (HST) is an ideal candidate for a wind turbine drivetrain. HST, a continuous variable transmission, has the advantage of delivering high power with a fast and accurate response. To evaluate the performance of the HST wind turbine, a power regenerative hydrostatic wind turbine test platform has been developed. A hydraulic power source is used to emulate the dynamics of the turbine rotor. The test platform is an effective tools to validate the control strategies of the HST wind turbine. This paper presents the high fidelity mathematical model of the test platform. The parameters of the dynamic equations are identified by the experiments. The steady state and transient operations results are compared with the experimental data. The detailed control architecture of the start-up and shut-down cycle is described for the test platform.

1 INTRODUCTION

Due to climate change and the need to decrease carbon dioxide emissions, there is a constant demand for green and renewable energy. Currently, renewable energy accounts for nearly 20% of the global energy usage. Within renewable energy, wind energy has seen the maximum growth since 2015 leading to rapid installation of wind turbines, worldwide, over the last decade. The US generates more than 4.5% of its total electricity from wind and has a goal of harnessing 20% of the nations energy from wind by 2030 [1].

Most utility scale wind turbines (greater than 1MW) are installed far away from the point of use, increasing transmission cost while incurring about 5% power loss in transmission lines. In contrast, for distributed wind, small (less than 100 kW) and midsize (100 kW to 1 MW) turbines can satisfy local demand and make the electrical grid more reliable and stable. Distributed wind can be used for industries, hospitals and communities. At present, distributed wind turbines are witnessing slow growth due to high costs of installation, operation and maintenance [2].

Hydraulic transmissions are used in applications where large torques are required, with fast response time and high accuracy [3]. Hydraulics are necessary for high power and high load applications such as construction equipment. The transmission consists of a hydraulic pump driving a hydraulic motor. For a continuous variable transmission (CVT), either the pump, or motor, or both need to have variable displacement. The dynamics of the HST are well studied in the past [4]. Hydraulic pumps and motors have power densities ten times higher than electric motors and generators, making the transmission more compact. The compressibility of hydraulic fluid reduces the impact loading on the mechanical components and increases the life of the transmission as compared to a gearbox [5]. As a CVT, an HST can adjust to varying wind speeds [6]. It rotates the generator at a constant speed and eliminates the need of an expensive power convertor (about 7% of total turbine cost). Commercial hydraulic components for HSTs in the required power range for midsize wind turbine are readily available at a reasonable cost.

To demonstrate and validate the performance of the HST, a unique power regenerative test platform has been built at the University of Minnesota [7]. The input to the HST drivetrain is the rotor torque. The rotor torque is computed from real wind profiles by using FAST code of National Renewable Energy Laboratory and emulated on the testbed using a hydrostatic drive (HSD) [8]. The output of the transmission is fed back to power the hydrostatic drive. It is a regenerative system which consumes less power to operate. The testbed is integrated with multiple sensors to accommodate and test a variety of hydraulic fluids, components and controls. To emulate the real rotor dynamics, fast and precise torque control is required for the hydrostatic drive. This research compliments the 1 MW HST wind turbine test platform research at RWTH Aachen University [9].

2 Power Regenerative Test Platform

The schematic of the power regenerative test platform is shown in Fig. 1. The system consists of three parts: a hydraulic transmission (HST) under investigation (block in dark grey), a hydrostatic drive (HSD) to emulate the rotor torque (block in light grey), and a control system (including a controller in Simulink environment in the host computer and real-time target computer). The rotor dynamics are simulated from the time varying wind profile and blade aerodynamics. Instead of dissipating the turbine output power, the power is fed back to the HSD. Because of power regeneration, the research platform is capable of generating 105 kW output with only 55 kW of electrical input. A variable frequency drive (VFD) is used to control the electrical input.

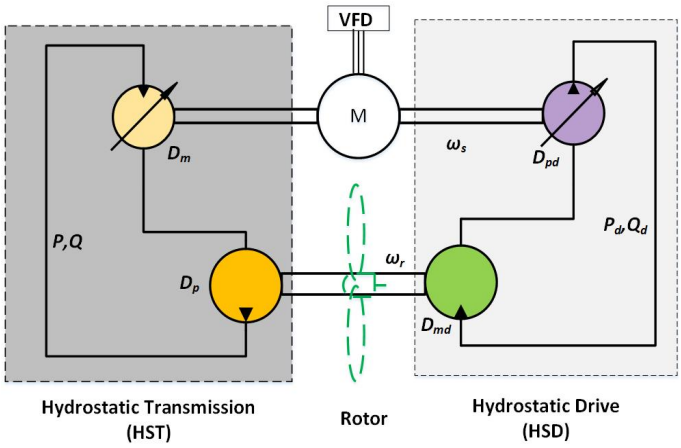

FIGURE 1. Schematic of Power Regenerative Testbed

The HST consists of a fixed displacement pump and a variable displacement motor. The rotor drives the fixed displacement pump creating the hydraulic flow. The pressurized hydraulic fluid is fed to the variable displacement motor driving the generator. The motor displacement is controlled by an electro hydraulic proportional valve. A boost pump is used to compensate for the fluid losses in the circuit as shown in Fig. 2.

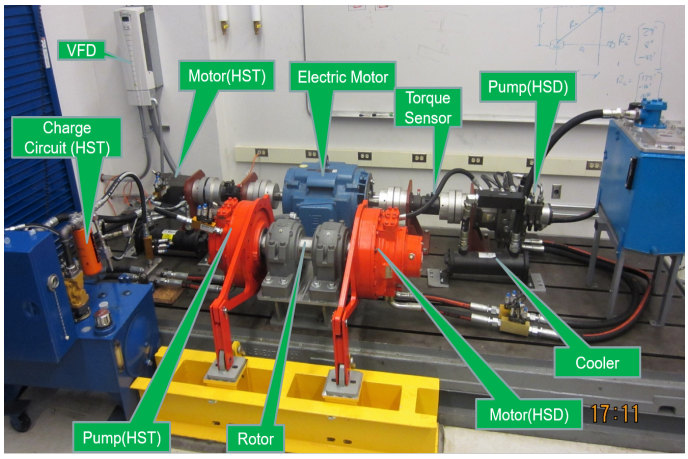

FIGURE 2. Power Regenerating Testbed

The HSD consists of a variable displacement pump and a fixed displacement motor. The electric motor along with the HST motor drives the variable displacement pump creating the hydraulic flow. The flow is controlled by an electro hydraulic proportional valve. The pressurized hydraulic fluid is fed to the fixed displacement motor driving the generator. The boost pump is integrated with the pump to compensate for the hydraulic losses.

The test platform has three control elements, electric motor current to control the high speed shaft speed, swash plate angle of the HSD pump to emulate rotor torque and swash plate angle of the HST motor to control the pressure of the HST for maximum energy capture.

3 Modeling of the Test Platform

3.1 High Speed Shaft Dynamics

The high speed shaft is driven by the hydraulic motor of the HST and the electric motor. A variable frequency driven electric motor is mounted on the turbine output shaft to make up for the losses of the HST and HSD. The electric motor also maintains the shaft speed at synchronous speed (1800 RPM) to emulate a four pole generator operating at 60 Hz grid frequency. The dynamics of the shaft is:

$$J_s\dot{\omega}_s + b_s\omega_s = \tau_e + \alpha D_m P - \chi D_{pd} P_d \quad (1)$$

J_s is the combined moment of inertia of shaft, HST motor and HSD pump and b_s is the damping coefficient of the shaft. The shaft is powered by the electric motor torque (τ_e) and the torque from the hydraulic motor of the HST (second term in right hand side). The shaft is loaded by the hydraulic pump of the HSD (third term on RHS). D_{pd} is the full displacement of the HSD pump, P_d is the pressure difference across the HSD pump, and $\chi(0,1)$ is the normalized swash plate angle of the HSD pump.

3.2 HSD Pressure Dynamics

The pressure in the control volume changes due to the difference between fluid entering and exiting the control volume. In the HSD, the pump creates the flow. Pressure builds up depending on the line load. Neglecting pressure losses and volumetric losses in the hydraulic hoses, the governing equation for the pressure is:

$$\dot{P_d} = \frac{\beta_{ed}}{V_d}\left[\chi D_{pd}\omega_s - D_{md}\omega_r - Q_{ld}\right] \tag{2}$$

The first term is the ideal flow from the pump, the second term is the ideal flow into the motor and the third term is the flow loss in the HSD system. V_d is the total volume of the pressure side, D_{md} is the displacement of the HSD motor, and ω_r is the angular speed of the hydraulic motor. The volumetric losses in the HSD motor are negligible and Q_{ld} is the leakage loss in HSD pump. The leakage loss is examined in section 4.

The effective bulk modulus β_{ed} is computed from bulk modulus of the fluid, β_f, bulk modulus of the hose, β_f, and adiabatic bulk modulus of the entrained air, $1.4P_d$ [10].

$$\frac{1}{\beta_{ed}} = \frac{1}{\beta_f} + \frac{1}{\beta_h} + \frac{s}{1.4P_d} \tag{3}$$

where, s is the percentage of entrapped air in the total volume. For the simulation, β_{ed} is linearized at operating pressure P_d.

3.3 Low Speed Shaft (Rotor) Dynamics

The power from the HSD motor is fed to the HST pump through the rotor. The dynamics of the rotor is governed by the following equation.

$$\begin{aligned} J_r\dot{\omega}_r + b_r\omega_r &= \tau_r(\omega_r, u, \phi) - D_p P \\ \tau_r &= D_{md}P_d\eta_{mmd} \end{aligned} \tag{4}$$

TABLE 1. System parameter in dynamic model

Symbol	Description	Value
D_{pd}	HSD Pump Displacement	180 cc/rev
D_{md}	HSD Motor Displacement	2512 cc/rev
D_p	HST Pump Displacement	2512 cc/rev
D_m	HST Motor Displacement	135 cc/rev
β_f	Bulk Modulus of the fluid	$1.8e^9 N/m^2$
β_h	Bulk Modulus of the hose	$1.12e^9 N/m^2$
V_d, V	Fluid Line Volume	$9.82e^{-4} m^3$
J_r	Moment of Inertia of Rotor	$2.17 Kgm^2$

where as J_r is the combined moment of inertia of the rotor and hydraulic pump. The rotor torque, τ_r, is a function of rotor angular velocity, ω_r, wind speed, u, and blade pitch angle, ϕ. b_r is the damping coefficient of the rotor shaft, D_p is the displacement of the hydraulic pump, P is the pressure difference across the pump and η_{mmd} is mechanical efficiency of the HSD motor. The mechanical losses of the radial piston HSD motor and HST pump are very small, so not accounted in the equation.

In the test platform, The hydraulic motor of the HSD emulates the aerodynamic torque on the rotor shaft. With the measured rotor speed and input wind speed and pitch angle, the torque is simulated in a hardware-in-the-loop (HIL) approach. The torque transient is created by controlling pump displacement of the HSD. The aerodynamic torque and HSD pressure relationship is shown in Eq. 4 .

3.4 HST Pressure Dynamics

The pressure dynamics of the HST system is similar to the pressure dynamics of the HSD and can be written as

$$\dot{P} = \frac{\beta_e}{V}\left[D_p\omega_r - \alpha D_m\omega_s - Q_{lt}\right] \tag{5}$$

where, β_e is the effective bulk modulus, V is the total volume of the pressure side, D_m is the displacement of the motor, $\alpha(0,1)$ is the normalized swash plate angle of the hydraulic motor, ω_s is the angular speed of the hydraulic motor, and Q_{lt} is the leakage losses in the hydraulic units.

The parameters of the test platform are listed in Tab. 1.

4 Identification of System Parameters

Unknown parameters of the power regenerative test platform are identified based on extensive experimental data.

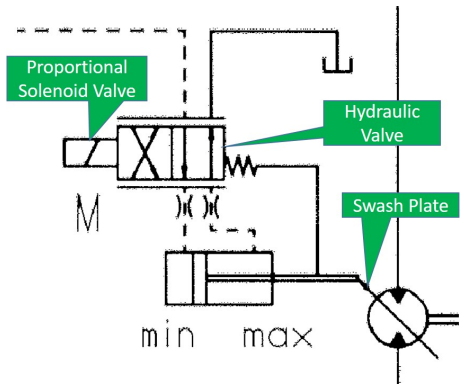

FIGURE 3. Mechanism for swash plate angle

Actuator: The HSD pump delivers the flow. At the constant speed operation, the flow from the pump can be varied by changing the swash plate angle . Similarly, the HST motor can operate at constant speed at different input flows by changing the swash plate angle. The swash plate angle is controlled by an electro hydraulic valve as shown in Fig. 3.

A proportional solenoid valve is used to change the position of the hydraulic valve, and the hydraulic valve controls the amount of fluid going into the cylinder, for controlling the cylinder position and hence the position of the swash plate. The proportional solenoid valve is controlled by the current, which is directly proportional to the applied voltage to the valve controller. The electro-hydraulic valve dynamics are ten times faster than the system bandwidth. So, the normalized swash plate angle of the HSD pump and HST motor can be modeled as linearly proportional to the applied voltage, shown in Eq. 6.

$$\begin{aligned} \chi &= K_d v_d \\ \alpha &= K_t v \end{aligned} \tag{6}$$

where, v_d and v are the input voltages of the valve controllers and K_d and K are the proportional gains for the normalized swash angles. The actuator outputs are limited and can be represented by a saturation function.

The HSD pump and HST motor do not have any sensor to measure the position of the swash plate. The HSD pump flow, Q_d, is measured to estimate the normalized swash plate angle ($\chi = Q_d/\omega_s * D_{pd}$). To reduce the internal leakage, the units are operated at high speed and low pressure. The estimated angle

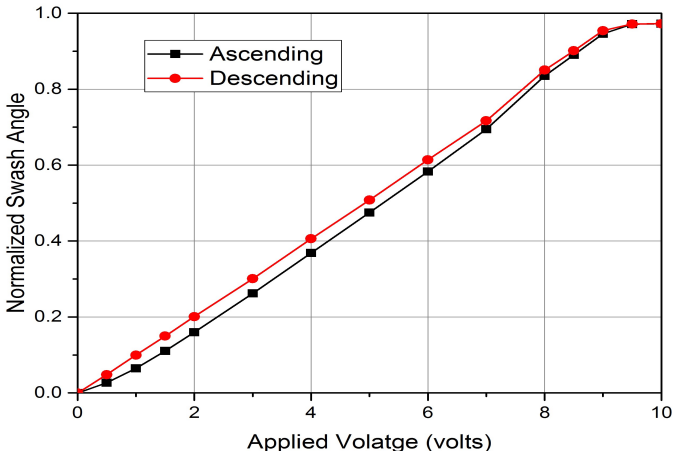

FIGURE 4. HSD normalized swash angle versus applied voltage

fraction versus the supplied voltage is shown in Fig. 4. The swash plate position has hysteresis and also saturates at a voltage above 9.3 Volt. The gain K_d, 0.107 is computed from the slope of the plot.

Similarly, the HST motor actuator gain is estimated from the input flow of the motor. The angle fraction versus the voltage is shown in Fig. 5. In contrast to the HSD pump, the HST swash angle does not have hysteresis or saturation. The normalized angle is linear with respect to the applied voltage and the gain K_t, is 0.093.

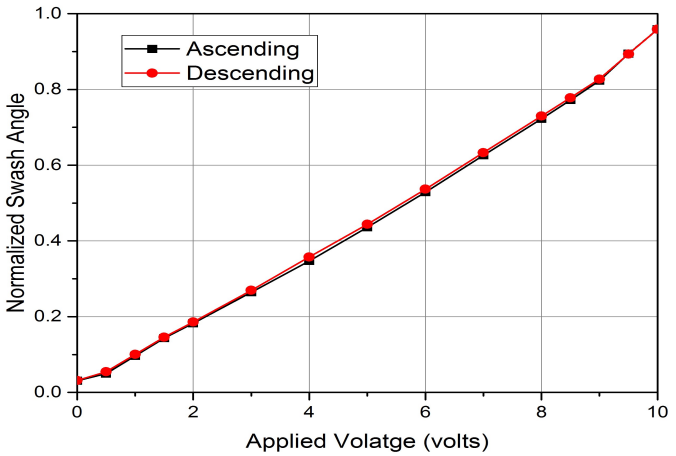

FIGURE 5. HST normalized swash angle versus applied voltage

Leakage Loss: The leakage loss of the radial piston HSD motor and HST pump are negligible. So, the flow loss Q_{ld} and Q_{lt} in Eq. 2 and 5 are related to the leakage loss in the HSD pump and HST motor. The leakage losses are internal flow losses

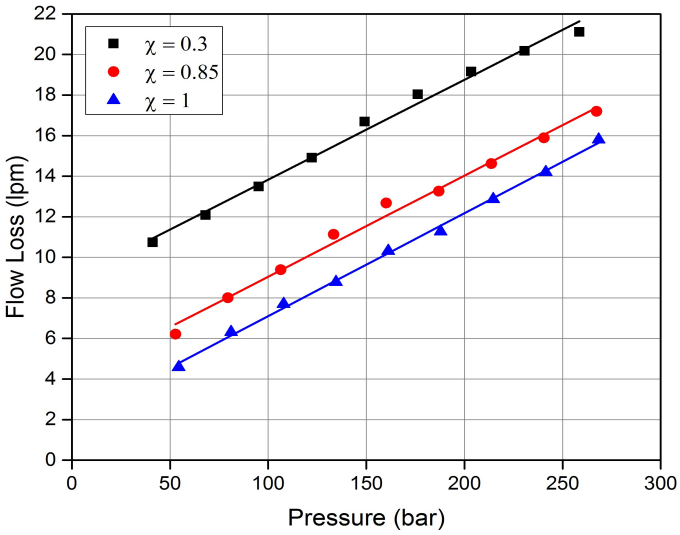

FIGURE 6. Flow losses versus pressure in the HSD

through the cylinder-piston gap and the port plate gap. The leakage flow increases with pressure and decreases with swash plate angle as shown in Fig. 6. The flow losses are measured and modeled as a linearly proportional to the pressure as shown below.

$$Q_{ld} = \omega_s D_{pd} - Q_{out} = L_d P_d$$
$$Q_{lt} = Q_{in} - \omega_s D_m = L_t P \quad (7)$$

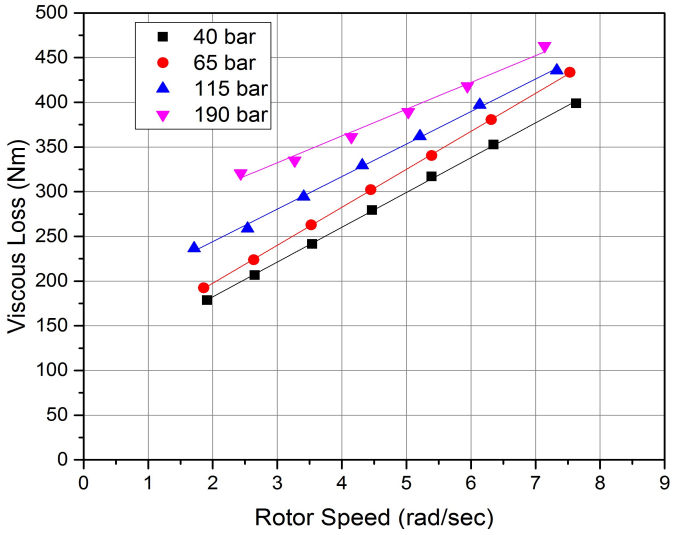

FIGURE 7. Viscous losses in the rotor

Based on experimental data, with least square fitting, the loss coefficient for the HSD pump, L_d is 0.049 lpm/bar and the HST motor, is L_d 0.010 lpm/bar.

Viscous Loss: The power from the HSD motor to the HST pump is transmitted through the rotor. The hydraulic units are mounted at both ends of the rotor and the rotor is supported by two bearings. The viscous friction losses in the bearings are directly proportional to the rotor speed.

From Eq. 4, at steady state, the viscous losses can be computed from the measurements of the rotor speed, ω_r, HSD pressure, P_d and HST pressure, P. The viscous loss in the rotor is shown in Fig. 7. The damping coefficient b_r is computed from the slope, which is 38.9324 Nm-sec. With an increase in the load, the viscous loss increases but the viscous coefficient remains the same.

Experimental validation: The developed model is validated with the experimental data. For the experiment, the HS shaft speed, ω_s is set to 1000 RPM and HST pressure, P is maintained at 100 bar. The swash plate angle of the HSD pump is varied in steps.

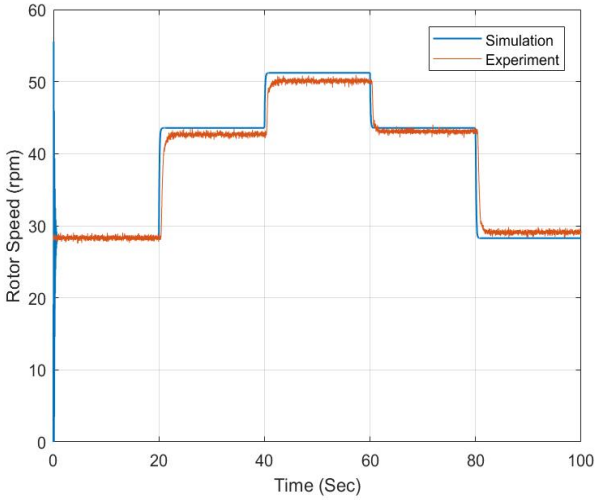

FIGURE 8. Comparison of the experimental and simulation data

Fig. 8, shows the rotor speed response for a step input of 4,6 and 7 volts (control command for HSD pump). At steady state, the experimental results match with the simulation data with a maximum steady state error of 2 RPM. In the transient case, the experimental data has slower response than the simulation data, since dynamics of the swash plate is not included in the simulation. In hardware in the loop experiments, we are going to emulate real rotor inertia, which is very high compared to the testbed rotor. Then the dynamics will be slower as compared to current experiments and simulation.

5 Controller Design

The overall control architecture of the power regenerative research platform is shown in Fig. 9. The research platform control system consists of the grid frequency simulator in the high-level control, an aerodynamic torque HIL simulator plus a HSD torque regulator in the mid level control and a drivetrain control system in the low level control.

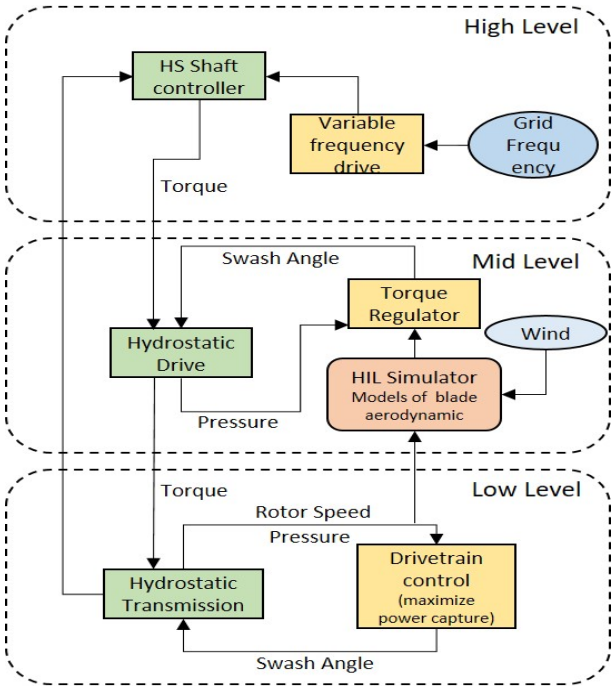

FIGURE 9. Control Architecture

In high-level control, the grid frequency is simulated by an electric motor and a VFD. The electric motor drives the HSD and controls the high speed shaft speed. The current to the electric motor is controlled through a 4 kHz pulse-width-modulation signal. Although the control dynamics of the VFD is fast, the acceleration of the electric motor is limited to reach synchronous speed of 1800 rpm in 20 sec. The high speed shaft response to a step input and ramp input is shown in Fig. 10. The steady state error to the step and ramp input is zero. The mid level control emulates the aerodynamic torque on the rotor from the wind. The HIL simulator is used to simulate the rotor torque from the wind input data and rotor speed. The rotor torque is then emulated on the test platform by controlling the swash plate angle of the HSD pump. The swash plate of the motor in the hydrostatic wind turbine drivetrain (HST) is controlled to optimize the power capture in the low level control. The power from the drivetrain is fed to the test platform to assist the electric motor to drive the HSD pump.

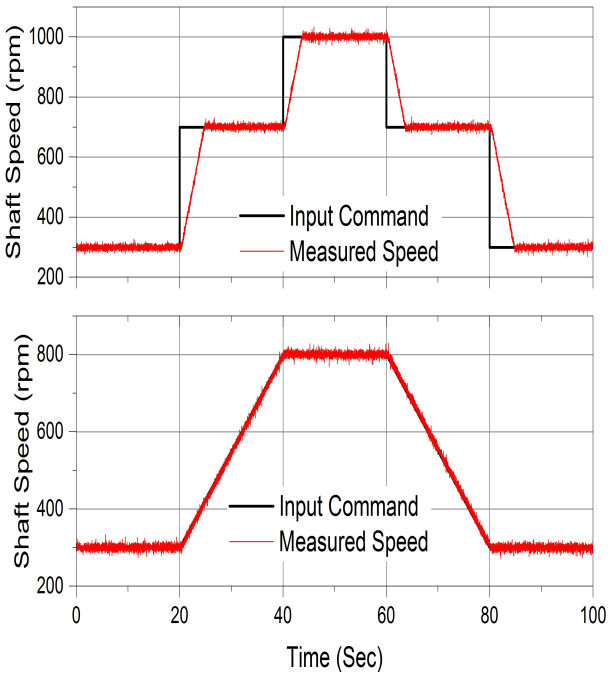

FIGURE 10. High speed shaft response

The test platform is controlled in three cycles, the start cycle, the test cycle and the stop cycle. The HSD and HST of the test platform are interconnected. So, the start and stop cycles are important for smooth operation and safety of the testbed. Particular attention is required to avoid caviataion and pressure spikes during these operations.

During the start cycle, the high speed shaft speed is brought to synchronous speed. To avoid cavitation, the HST motor displacement is set to zero, the electric motor is set to 100 RPM and the HSD pump is set to half displacement, to create flow to drive the rotor. In some cases, the HSD pump flow recirculates internally and does not have sufficient power to drive the rotor. In that case, the electric motor speed increases until the rotor starts rotating. As soon as the rotor rotates, the HST pump creates flow and the pressure starts building up in the HST line. The swash plate angle of the HST motor is controlled to reduce the pressure. Once the pressure of the HST is greater than 40 bar and less than 100 bar and its displacement is more than half of the full displacement, the electric motor is ramped up to synchronous speed in steps of 500 RPM. The detailed architecture is shown in Fig. 11.

The research platform is governed by four dynamic equations, with four states, ω_s, ω_r, P_d and P, and three inputs v_d, v and τ_e, as shown in Eq. 1- 5. In Eq. 1, 2 and 5, the states are multiplied with inputs and have non-linear dynamics. However, In the test cycle, the high speed shaft rotates at synchronous speed, meaning that ω_s is fixed. The dynamics of the research plat-

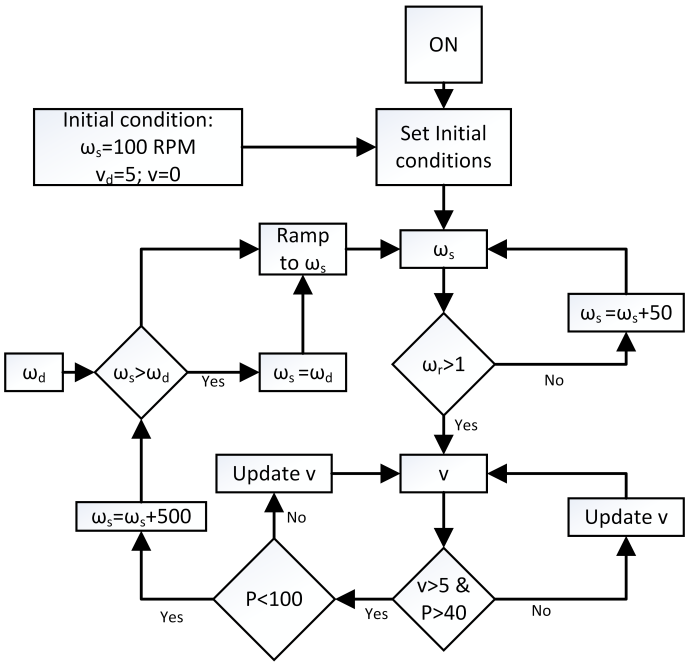

FIGURE 11. Start up flowchart

form is regulated by Eq 2- 5. The dynamics became linear with constant synchronous speed. The mid and low level controllers are designed to regulate the HSD pressure, to emulate the rotor torque and HST pressure to optimize the power capture.

In the stop cycle, the high speed shaft speed is brought to rest from synchronous speed. At first, the HST pressure is reduced to 50 bar, and then the electric motor speed is ramped down to 200 RPM. Then, the HST pressure is reduced to 30 bar and the electric motor speed is brought down to zero for smooth stopping.

CONCLUSIONS

In this paper, the mathematical models of the power regenerative test platform have been derived. The unknown parameters of the test platform, such as swash plate angle gain, pressure loss coefficients of the hydraulic units and the damping coefficient of the rotor are identified from extensive experiments. The mathematical model is compared with the experimental data. The control objectives of the research platform are discussed here. The start-up and stop procedures are laid out for smooth operations, without creating cavitation in the HST. Overall, this dynamics will provide a greater insight to the behaviour of the research platform and also will help us to develop the mid level and low level controllers in the future.

ACKNOWLEDGMENT

This project is funded by the National Science Foundation under grant 1634396. We also thank Eaton, Linde, Danfoss, Bosch Rexroth, Flo-tech and ExxonMobil for donating the components for the test bed. We are thankful to our other graduate students in our lab for helping us in setting up the experiments.

REFERENCES

[1] Wind vision report by united states department of energy. https://energy.gov/eere/wind/wind-vision.

[2] Distributed wind market report by united states department of energy. https://energy.gov/eere/wind/downloads/2015-distributed-wind-market-report.

[3] Schmitz, J., Diepeveen, N., Vatheuer, N., and Murrenhoff, H., 2012. "Dynamic transmission response of a hydrostatic transmission measured on a test bench". In Innovating today shaping tomorrow: Scientific proceedings of the European wind energy conference and exhibition (EWEA 2012), Copenhagen, Denmark, 16-19 April, 2012, Citeseer.

[4] Manring, N., and Luecke, G. R., 1998. "Modeling and designing a hydrostatic transmission with a fixed-displacement motor". *Journal of dynamic systems, measurement, and control,* ***120***(1), pp. 45–49.

[5] Thul, B., Dutta, R., and Stelson, K. A., 2011. "Hydrostatic transmission for mid-size wind turbines". In Proceedings of 52nd National Conference on Fluid Power, Las Vegas, NV, pp. 443–458.

[6] Dutta, R., Wang, F., Bohlmann, B. F., and Stelson, K. A., 2014. "Analysis of short-term energy storage for midsize hydrostatic wind turbine". *Journal of Dynamic Systems, Measurement, and Control,* ***136***(1), p. 011007.

[7] Mohanty, B., Wang, F., and Stelson, K. A. "Design of power regenerative hydrostatic wind turbine test platform". *"Proceedings of the 10th JFPS International Symposium on Fluid Power Fukuoka, Japan, Oct 2017"*.

[8] Jonkman, J. M., and Buhl Jr, M. L., 2005. Fast user's guide-updated august 2005. Tech. rep., National Renewable Energy Laboratory (NREL), Golden, CO.

[9] Schmitz, J., Vatheuer, N., and Murrenhoff, H., 2011. "Hydrostatic drive train in wind energy plants". *RWTH Aachen University, IFAS Aachen, Germany*.

[10] Manring, N., 1997. "The effective fluid bulk-modulus within a hydrostatic transmission". *Journal of dynamic systems, measurement, and control,* ***119***(3), pp. 462–466.